Composite Structures 265 (2021) 113744

Contents lists available at ScienceDirect

Composite Structures

journal homepage: www.elsevier.com/locate/compstruct

Conductive 3D printed PLA composites: On the interplay of mechanical, electrical and thermal behaviours

I. Tirado-Garcia [a], D. Garcia-Gonzalez [a,*], S. Garzon-Hernandez [a,b], A. Rusinek [c,d], G. Robles [e], J.M. Martinez-Tarifa [e], A. Arias [a,*]

[a] Department Continuum Mechanics & Structural Analysis, University Carlos III of Madrid, Avda. Universidad 30, Leganés 28911, Madrid, Spain
[b] Current affiliation: Department of Engineering Science, University of Oxford, Parks Road, Oxford OX1 3PJ, UK
[c] Laboratory of Microstructure Studies and Mechanics of Materials, UMR-CNRS 7239, Lorraine University, 7 rue Félix Savart, BP 15082, 57073 Metz Cedex 03, France
[d] Chair Excellence, Dpto. Ingeniería Mecánica, U. Carlos III of Madrid, Avda. Universidad 30, 28911, Leganés, Madrid, Spain
[e] Department of Electrical Engineering, U. Carlos III of Madrid, Avda. de la Universidad 30, 28911, Leganés, Madrid, Spain

ARTICLE INFO

Keywords:
Additive manufacturing (AM)
Conductive Polymer Composites (CPC's)
Fused deposition modelling (FDM)
Carbon black (CB)
Polylactic acid (PLA)
Multifunctional materials

ABSTRACT

Additive manufacturing (AM) techniques represent a real challenge to manufacture novel composites with coupled multifunctional properties. This work focuses on the mechanical, electrical and thermal behaviours of 3D printed polymeric composites of polylactic acid (PLA) filled with carbon black (CB) conductive particles. The incorporation of conductive particles within the polymer matrix allows for programmable conduction paths via the printing process, whose electric properties are intimately coupled to thermo-mechanical processes. In this study, samples were prepared using a fused deposition modelling (FDM) printer, controlling the filament orientation to manufacture three different types: longitudinal (0°); transverse (90°); oblique (±45°) printing orientations. Different types of multifunctional characterisation have been made: (i) electro-thermal tests, evaluating the influence of electrical conductivity on the sample temperature due to Joule's heating; (ii) thermo-electrical tests, analysing the influence of temperature on the DC resistance of the samples; (iii) mechano-electrical tests, analysing the effect of mechanical deformation on the specimens' electric resistance. The results show a strong dependence of printing direction on the material properties of 3D printed conductive-PLA and identify strong thermo-electro-mechanical interplays. The results of this work will contribute to the AM progress in functional electro-mechanical components with potential applications in biosensing devices, composite sensors, 3D electrodes and soft robotic industry.

1. Introduction

Additive manufacturing or three-dimensional (3D) printing technologies have revolutionised the field replacing traditional manufacturing processes. These technologies have opened the door to versatility in design, allowing for the customisation of structural components [1–5], while decreasing the cost and cyclic times with simpler supply chains [6,7]. The printing advancements experienced in the last decades and their use have been extended to a wide variety of fields such as automobiles, medical implants, electronics, aerospace and robotics [5,7,8–11]. More recently, this concept has moved to the so called 4D printing technology [7,12,13]. The latter consists in manufacturing polymeric components controlling not only the structural features but also other functionalities with at least one property that varies in space and/or time [13]. Among them, it is worth mentioning polymers with thermo-active [1,14], photo-responsive [5], electro-active [15] or magneto-active responses [16–18]. All these responsive polymers share the ability to mechanically response to an external stimulus by adapting their shape or mechanical properties (i.e., material stiffness). A special type of 4D printed polymer are conductive polymeric materials. These present higher intrinsic electrical conductivity thanks to the incorporation of conductive particles within the polymeric matrix. Conductive polymers have been classified as promising candidates in different applications such as flexible electronics [10,19], energy storage [5], bioelectronics [20,21] or tissue engineering [12,22].

The mechanical properties of the matrix determine the microstructural features of the composite, its stiffness, strength or ductility. Thus, it is possible the fabrication of soft conductive 3D printed polymers by using polymeric matrices in dry or hydrogel states. In this regard, Zhao

* Corresponding authors.
E-mail addresses: danigarc@ing.uc3m.es (D. Garcia-Gonzalez), aariash@ing.uc3m.es (A. Arias).

https://doi.org/10.1016/j.compstruct.2021.113744
Received 18 December 2020; Revised 11 February 2021; Accepted 14 February 2021
Available online 23 February 2021

and co-authors have recently published some works where developing 3D printing manufacturing techniques for rapid and flexible fabrication of highly conductive microscale structures and devices [23,24]. These works offer a pioneering fabrication strategy to design and manufacture bioelectronics, wearable devices, and flexible electronics based on conductive polymers. Other possibility is to use thermoplastic polymers for the composite matrix. In this regard, the resulting component suffers of lower ductility and flexibility but offers higher structural integrity. These thermoplastic materials can be filled by conductive nanoparticles that are distributed forming conductive paths for the charge transport. By producing these composites in the form of filaments, they can be 3D printed by fused deposition modelling (FDM). In this regard, conductive polymer composites (CPCs) manufactured by FDM offer versatility to 3D print electrical circuits and components, allowing for a wide range of combinations between matrix and functional filler [13]. Some recent works have explored the suitability of these 3D printed conductive polymers employing as matrix ultra-high molecular weight polyethylene (UHMWPE) [25], nylon–6 or polyethylene (PE) [26], polyurethane [19] or Polylactic acid (PLA) [27,28].

From a mechanical perspective, the behaviour of the thermoplastic component, even in the absence of the conductive particles, is highly complex. In this regard, most of these thermoplastics present strong nonlinearities, viscous relaxations, strain rate dependences, thermal softening and thermal transitions [29–32]. Moreover, when the thermoplastic polymer is manufactured by FDM, additional complexities are incorporated to the mechanical response such as anisotropy induced by filament deposition orientation, or the inclusion of anisotropic porosity [33,34]. In addition, the final material performance depends on the printing conditions, i.e., extrusion temperature, layer height, printing speed [2,35,36]. In the case of 3D printed thermoplastic polymers filled with conductive fillers, the manufacturing conditions play a double role. On the one hand, the printing conditions influence the mesoscopic structural characteristics of the material, as they govern the sintering process that determine the interfilament bonding and, therefore, the composite porosity [2,3]. Moreover, one of the challenges is optimizing the volume of the filler fraction in the matrix. This must be sufficient to ensure the dielectric transition to conductor but not too high to lead to clogged nozzles and brittle filaments [13,37]. On the other hand, the dispersion of the conductive fillers within the polymeric matrix establishes the potential pathways for the charge conduction. Therefore, a good sintering process is essential to allow for jumping from filament to filament and favour the composite conductivity. Among the different CPCs, polymeric filaments with carbon black (CB) as filler are the ones that arouse the most interest due to their easy availability and low cost [6,13,20]. In very recent works, Abdalla et al. [38] evaluated the influence of different printing parameters on the resistivity of the CB/PLA composites; Kim and Lee [39] analysed the electrical heating of honeycomb CB/PLA structures. These studies confirmed electrical and heating characteristics, but not mechanical considerations have been made [40].

Although there are some published works exploring the electrical or mechanical response of 3D printed CPCs, to the authors' knowledge, there are no studies that have addressed this problem accounting for different physical interlinks. In this regard, the electrical conduction depends on the maintenance of physical pathways via interconnexion of conductive particles' aggregates (i.e., CB particles). Hence, the electrical response is intrinsically coupled to mechanical deformation, as the deformation of the polymeric matrix implies changes in the relative position of the conductive particles. In addition, the presence of an electric current leads to temperature increase due to Joule's heating. In turn, this temperature increase results into thermal expansion of the polymeric matrix as well as mechanical softening. Therefore, the overall behaviour of 3D printed conductive polymers needs to account, in a coupled manner, for thermal, electrical and mechanical behaviours.

Motivated on the previous statements, this work aims at evaluating the interplays between thermal, electrical and mechanical responses of 3D printed PLA reinforced with CB particles (CB/PLA) manufactured by FDM. The filament orientation is controlled during the manufacturing process to provide three different types of samples: longitudinal (0°), oblique (±45°), and transverse (90°) printing orientations. To this end, experiments are conducted to study different couplings: (i) electro-thermal tests, evaluating the influence of electrical conductivity on the sample temperature due to Joule's heating; (ii) thermo-electrical tests, analysing the influence of temperature on the DC resistance of the samples; (iii) mechano-electrical tests, analysing the effect of mechanical deformation on the specimens' resistance. The results from this study show the consequences of incorporating conductive particles within the composite by means of mechanical performance and electrical conductivity. In addition, a strong dependence of printing parameters on the material properties of 3D printed CB-PLA is observed and we identify strong thermo-electro-mechanical interplays. The results of this work will contribute to the AM progress in functional electro-mechanical components.

2. Conductive 3D printed polymeric composite: PLA filled with carbon black particles

2.1. Baseline material

The composite material used in this study is a commercial polylactic acid/carbon black [41], based on a polymeric matrix of PLA 4043D reinforced with CB particles (53% of CB by mass and 26.5% by volume, with a median particle size by volume of 224 μm) [38]. The PLA is a thermoplastic semi-crystalline polymer widely employed in FDM additive manufacturing [5,22,27]. Carbon Black particles are obtained with the incomplete combustion of petroleum derivatives and, currently, is one of the most used nanomaterials as a reinforcement of rubber and polymers due to its versatility and its very high surface/volume ratio [20]. In addition, these particles combine these characteristics with a predominant content of conductive type of carbon, which favours the particles' aggregation within the polymeric matrix forming conductive pathways within the composite [38,39]. Therefore, the filament form of the CB-PLA allows for its manufacturing by FDM printing providing a low resistivity semiconductor. The many applications of this material can be found in many industrial and research sectors. Some examples are, among others: tissue engineering [22], biosensors [21], electrodes for detection [42], antistatic application [43], soft actuators [19], electrical circuits [13], composite wires [44], thermoelectric components [14] and capacitive sensor [20]. Other applications are Faraday boxes that isolate from electromagnetic waves, fuses with complex geometries, resistors for electronic circuits and customized prostheses that allows for transmission and/or reception of electrical currents [13,45].

2.2. 3D printing manufacturing process

During previous works with FDM printed polymers we observed that, in agreement with the literature [46,47], the dogbone geometry of the specimens caused premature failure due to stress concentration in the radius of the fillet for 3D printed samples [2]. To alleviate this issue, thin rectangular specimens are used instead, providing good mechanical response during tensile testing. Following these previous observations, specimens were printed with a size of 165 mm × 13 mm × 3 mm. The simplification of such a rectangular geometry also helps at imposing and analysing the electric response.

The main aim of this work is to study the interplays of mechanical, electrical and thermal effects on 3D printed conductive polymers. To this end, we fix most of the printing parameters to default values and only change the filament orientation to further study this influ-

ence on the formation of conductive pathways. Therefore, the fixed printing parameters used in all the specimens' manufacturing are: road width of 0.4 mm, layer height of 0.2 mm, air gap of 0 mm, printing temperature of 230 °C, build plate temperature of 60 °C, infill density of 100%, printing speed of 30 mm/s, and a single contour was deposited along the component edge [48]. Moreover, the filaments were deposited following a same pattern within the specimen, determined by the filament direction. In this regard, three filament directions were considered: longitudinal (0°), oblique (±45°) and transverse (90°) printing orientations.

2.3. Microstructural characterisation

This section introduces an analysis on the microstructural arrangement of the conductive particles (i.e., CB particles) within the polymeric matrix. This microstructural arrangement fully determines the nature of the electrically conductive behaviour of the 3D printed CB-PLA. In this regard, due to the dielectric characteristic of the polymeric matrix, the conduction of the electric current directly depends on the distribution of the CB particles inside. As shown in the schematic representation of Fig. 1, the conduction of the electric current and, therefore, the resistivity of the material depends on the formation of CB aggregates forming electric paths within the composite. These electric paths will be formed at two levels: i) at the filament level, providing electric conduction along the filament direction; ii) at the interfilament level, providing electric conduction between different filaments. These features and the differences between the formation of electric paths within and between filaments thus determine the suitability of the conductive composite and the influence of the printing direction.

The first analysis performed here aims at evaluating the microstructure of the 3D printed PLA 4043D without CB particles inclusion and of the 3D printed CB-PLA. In addition, we evaluate the distribution of the CB particles within the filament before and after 3D printing. To this end, scanning electron microscope (SEM) images were taken, Fig. 2. When comparing the mesostructure of the printed PLA and the printed CB-PLA, important differences are observed. For the PLA specimen without conductive particles, a good sintering process occurs leading to a good interphase between filaments. However, when the conductive particles are filled within the PLA matrix, the sintering process is affected negatively leading to a worse interphase between filaments and a considerable increase of porosity. This effect can be explained by a higher limitation in polymeric chains' mobility due to the presence of the particles.

Moreover, other than the mesoscopic porosity of the composite, the microstructural arrangement of the conductive particles within the polymeric matrix is of most importance. As shown in Fig. 1, the internal distribution of the particles and the aggregates formed determine the electrically conductive behaviour of the composite. Therefore, we analysed the influence of the printing process on the microstructural distribution of the particles. To this end, SEM images (Fig. 2) were taken on a filament before printing and on a printed specimen. The results showed the same aggregation patterns and suggested that the differences in the electric conductivity of the material will be determined by the sintering process between filaments rather than specific microstructural arrangements. Within the filaments, a homogeneous distribution of the filler is observed in both pre-printed and 3D printed filaments.

In addition, we complemented the microstructural characterisation by analysing the composition of the material after 3D printing. This analysis was conducted by SEM and provided the composition analysis within a total area of 230 μm^2 and local measurements. These results showed a composition with high concentration of carbon (89.62%), a slight concentration of sulphur associated to a dispersant (0.11%), and the presence of oxygen associated to the molecular structure of PLA (10.26%).

3. Interplay between thermal and electrical responses

This section aims at evaluating the bidirectional coupling between thermal and electrical responses. To this end, we first performed experimental tests analysing the temperature evolution due to the application of a constant electric potential on a printed conductive specimen. Then, we inverted the problem and analysed changes in electric resistance due to heating and cooling processes.

3.1. Electric effects on composite temperature

We evaluated the effects of applying a constant electric potential on the three different 3D printed conductive specimens. This study is motivated by Joule's heating due to the resistive nature of the CB-PLA [39,49]. We hypothesise that the electric resistance of the material directly depends on the formation of the conductive paths by CB aggregates. According to the analysis performed in Fig. 2, the distribution of the conductive particles within the printed filaments can be assumed homogeneous, leading to *a priori* constant resistivity along the filament orientation. However, the overall resistance of the specimen will also be highly influenced by the printing orientation of the filaments and the resulting sintering process. Therefore, to study these potential dependences of the electro-thermal coupling, we performed experiments where a constant electric potential (30 V under DC conditions) is applied longitudinally in specimens printed with different filament orientations: longitudinal (0°), oblique (45°/−45°), and transverse (90°). The heating process is characterised using an infrared camera that measures the surface temperature along the sample. This allows to detect not only an overall increase of the samples' temperature, but also potential inhomogeneities in the temperature distribution as well as to determine the temperature of the hottest area. The results for these experiments are shown in Fig. 3.

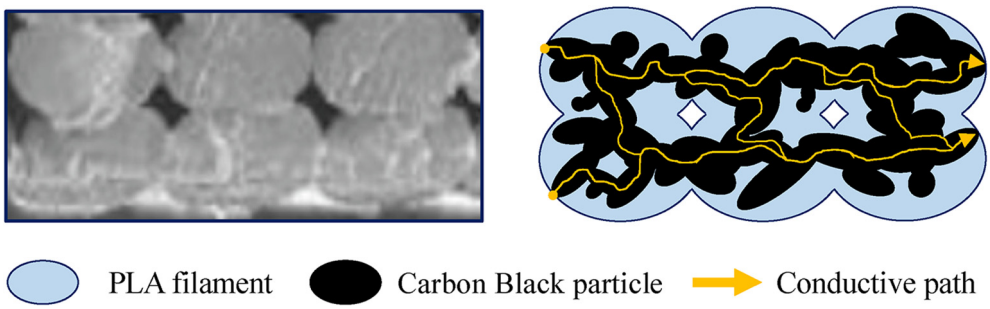

Fig. 1. Scheme of the microstructural composition of the 3D printed CB-PLA. It can be observed the nature of the conductive electric response related to the formation of CB pathways within the composite. In the left-hand side, the SEM image corresponds to a local region of a printed specimen with road width of 0.4 mm and layer height of 0.2 mm.

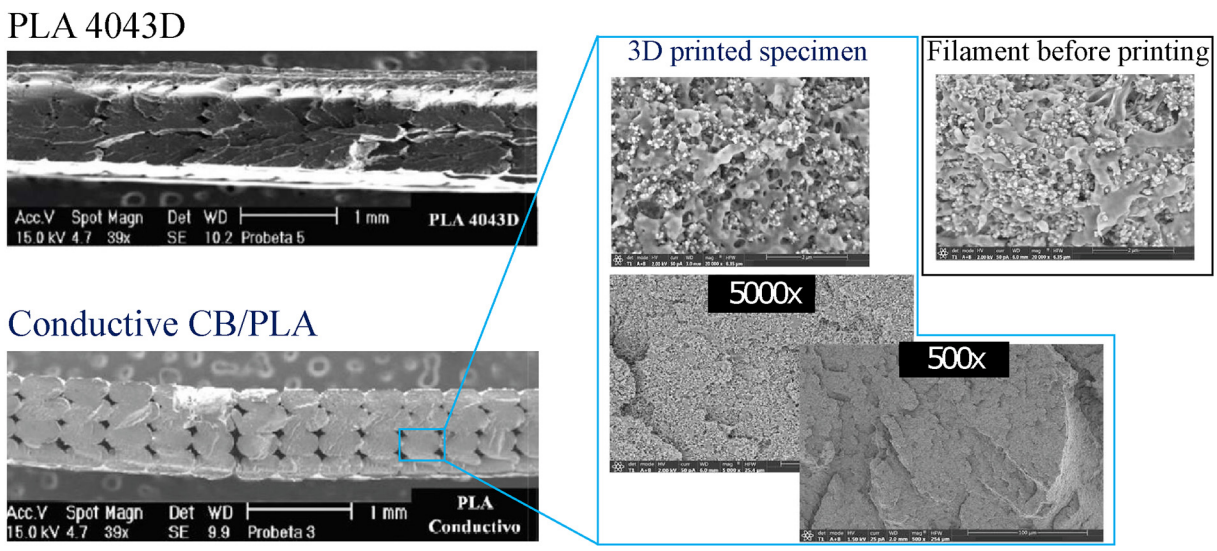

Fig. 2. Left: SEM images of printed PLA and printed CB-PLA. Right: Zoom-in SEM images of the microstructure of CB-PLA after printing (3D printed specimen), and SEM image of CB-PLA before printing (Filament before printing).

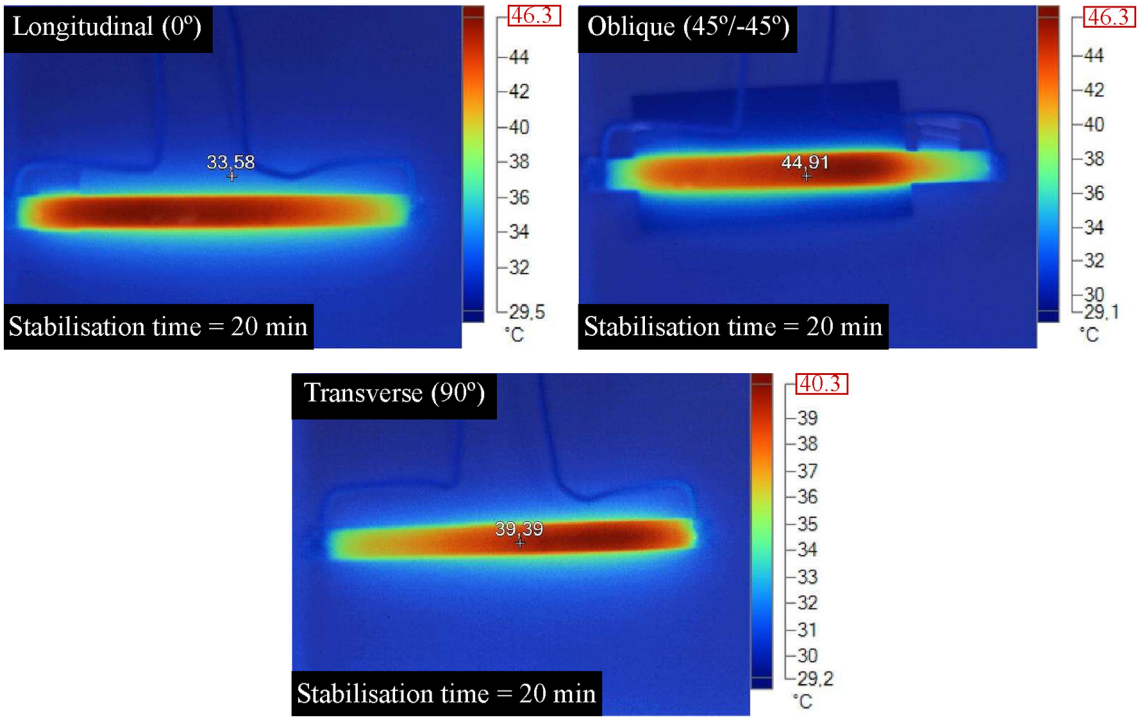

Fig. 3. Temperature distribution within 3D printed CB-PLA specimens due to the application of a constant field of 30 V (DC) and the consequent Joule's effect. Three different printing orientations are used: longitudinal (0°); oblique (45°/−45°); transverse (90°). Each case is presented highlighting the maximum local temperature reached and the stabilisation time. The latter refers to the time at which temperature shows stabilization (changes below 0.5 °C between consecutive measurements).

Overall, it can be noted an increment in temperature due to the resistive nature of the material and the associated Joule's heating. An important observation is that there are significant differences in the distribution of the temperature within the specimen depending on the filament printing direction. In this regard and for the specimen geometry employed, the longitudinal (0°) specimens showed a relatively homogeneous distribution of temperature increase. This distribution becomes more heterogeneous when increasing the printing angle with respect to the longitudinal orientation of the specimen geometry. Thus, the temperature distribution seems to turn to slightly heterogeneous for oblique (45°/−45°) specimens and to more heterogeneous for transverse (90°) specimens. These results can intuitively be explained by the formation of conductive paths. For the longitudinal specimens, the electric current follows conductive paths formed within the filament printing direction. Therefore, there is no such an importance of the formation of conductive paths through filaments sintering. However, as the printing direction is highly misaligned with the conduction direction, the conductive paths formed between filaments become more important in the charge transport mechanism. These conductive paths are much more heterogeneous as depend on

the local sintering process and are more likely to present material defects, which hinders charge transport (and the corresponding current flow) along the samples. These features altogether lead to local heterogeneities of resistivity within the composite, resulting into higher heterogeneities in temperature increase due to Joule's effect.

When the constant electric potential of 30 V under DC conditions is imposed on the specimens, another relevant analysis arises from the evolution of temperature along time depending on the filament orientation. For this, we show the evolution of the maximum local temperature reached in each specimen at each time, see Fig. 4. All specimens present a similar tendency: an important increase of temperature that stabilises at a characteristic time (hereafter, stabilisation time). This response is due to the competition of two thermal processes. The first one is related to the resistive nature of the specimen that, under the presence of an electric current, leads to temperature increment due to Joule's effect. The second process relates to convection terms due to the difference in temperature between the sample and the surrounding medium. As a consequence of the combination of both effects, the temperature within the specimen increases until reaching a thermal equilibrium with the environment (room temperature). When comparing the three different specimen configurations, it can be observed higher temperature increases for longitudinal printing orientation and lower ones for transverse orientations. The oblique specimens present temperature increments between longitudinal and transverse ones, although the stabilisation temperature is the same than the one for longitudinal specimens (note that stabilisation time is higher though). These results are explained by the direct relation between generated heat due to Joule's effect, Q, and the specimen resistance, R, computed as (Fig. 5):

$$Q = \int \frac{V^2}{R} dt \tag{1}$$

where V is the electric potential and t is the time variable. Note that the electric potential is imposed constant along the test (30 V). Therefore, higher temperatures are expected for specimens with lower resistance R. This is consistent with the discussion presented in this section and the results provided in next section, which show lower resistance for longitudinal specimens and higher ones for transverse specimens.

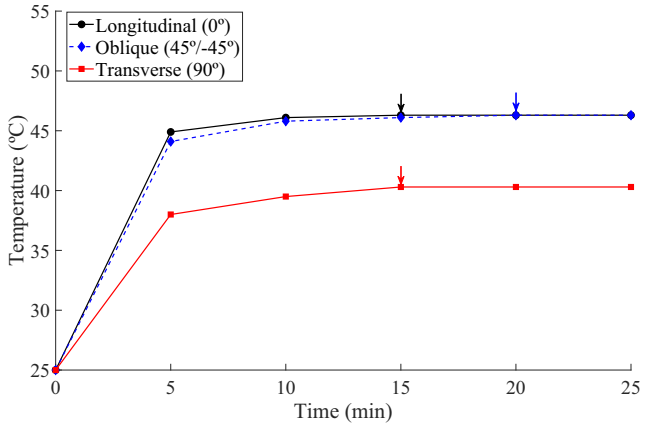

Fig. 4. Temperature evolution with time for 3D printed CB-PLA specimens subjected to the application of a constant field of 30 V (DC) and the consequent Joule's effect. Three different printing orientations are used: longitudinal (0°); oblique (45°/−45°); transverse (90°). The temperature corresponds to the maximum local temperature reached at each time. The arrows point the stabilization time (changes below 0.5 °C between consecutive measurements).

3.2. Thermal effects on composite resistance

This section aims at complementing the electro-thermal analysis presented above by evaluating the inverse coupling, i.e., thermo-electrical [14,50,51]. To this end, we evaluated the effects on electric resistance of applying heating and cooling rates on the three different 3D printed conductive specimens. This analysis not only considers changes in resistance due to temperature changes themselves, but also due to mechanical deformations associated to thermal expansion. To conduct such experiments, we conducted experiments in parallel for the three specimen configurations used (longitudinal, oblique and transverse). The 3D printed CB-PLA specimens were placed into a thermal chamber that applied heating until reaching the targeted temperature values. The temperature was monitored by the thermocouple of the chamber and by an extra thermocouple located close to the specimens to ensure homogeneous conditions within the chamber. Three conventional ohmmeters were used to measure resistance from the three different specimens online with the temperature. These ohmmeters apply lower voltages to the samples, unable to heat them by Joule's effect, such as the voltage levels applied in Section 3.1.

The results of heating experiments are presented in Fig. 6. Overall, we observed lower resistance for longitudinal specimens and higher resistance for transverse ones, with oblique specimens presenting intermediate values. This is explained by the nature of the main conductive paths used by the electric current, which follows paths within the filaments in the longitudinal specimens and interfilament paths for the oblique and, especially, transverse specimens. This is consistent with the aforementioned heating mechanism observed as a consequence of Joule's Effect. Thus, in the oblique and transverse specimens the resistance does not depend uniquely on the dispersion of conductive particles' aggregates but also on the sintering process that promotes the formation of conductive paths between filaments. According to the microstructural characterisation, see Fig. 2, the sintering process does not develop in optimal conditions resulting in high porosity. The presence of such porous along the current direction together with material defects within the interfilament region explain the higher resistance presented in transverse specimens. Moreover, all the printed specimens, independently of the printing filament direction, show the same trends by means of resistance evolution with temperature. In this regard, all specimens present a plateau region ("1" in Fig. 6) where the electric resistance is almost constant (from room temperature to around 37 °C). In this region, the composite maintains the microstructure experiencing only some thermal expansion. For higher temperatures ("2" in Fig. 6), the thermal expansion leads to large enough deformations of the composite resulting in the rupture and/or alteration of the conductive paths. This results into a significant increase in resistance with temperature, that becomes stronger when reaching the glass transition of the polymeric matrix (65 °C). In this region, the polymeric chains present higher mobility and it translates into an important increase in resistance-temperature slope. However, this tendency is turned at around 75 °C showing a decrease of resistance with temperature ("3" in Fig. 6). We hypothesise here that this changed in the tendency is due to the higher mobility of the microstructural phases that leads to the formation of new electric conductive paths. Finally, this trend changes again to positive resistance-temperature slope due to thermal expansion and the subsequent disruption of conductive paths ("4" in Fig. 6). Note that resistivity changes with temperature for CB particles are negligible compared with the changes observed during these tests. A quantitative comparison between the three specimens' configurations is provided by means of the resistance versus temperature slopes $\left(\frac{dR}{dT}\right)$ within the plateau region ("1" in Fig. 6). The longitudinal specimens (0°) present an average $\frac{dR}{dT} = 4.3\ \Omega/°C$, the oblique specimens (45°/−45°) present an average $\frac{dR}{dT} = 4.4\ \Omega/°C$, and the transverse specimens (90°) present an average $\frac{dR}{dT} = 6.5\ \Omega/°C$. These results suggest again the importance of

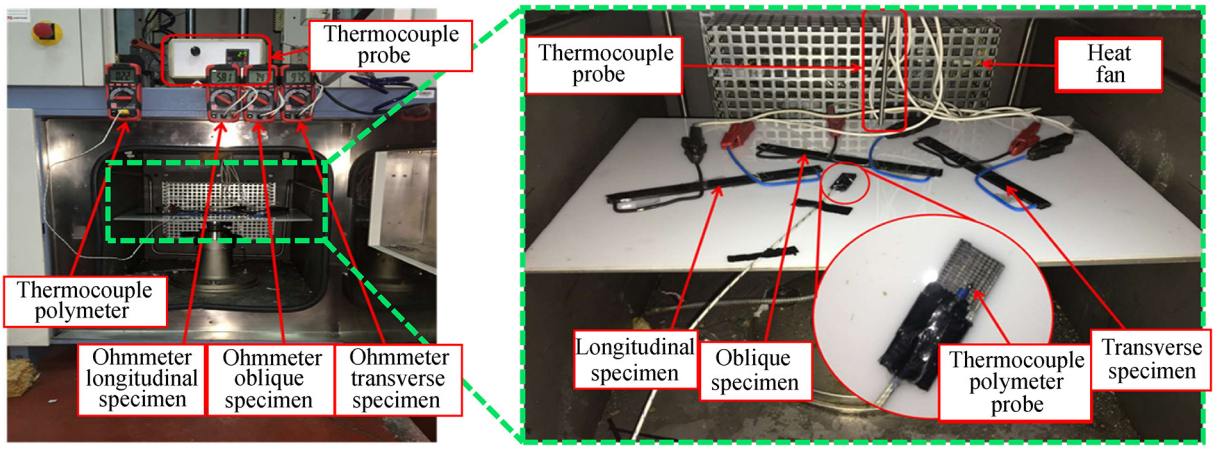

Fig. 5. Experimental setup for testing the influence of temperature on the resistance of 3D printed conductive specimens.

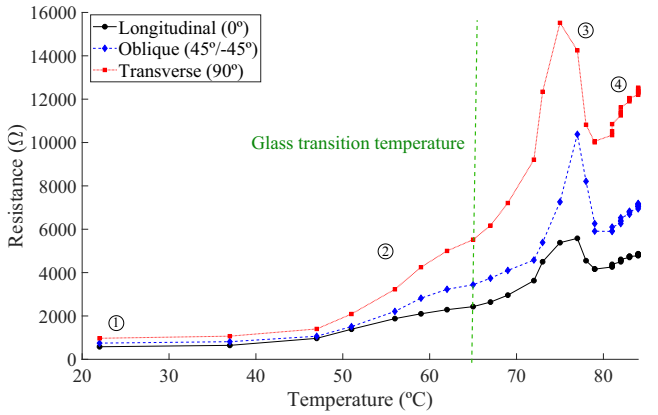

Fig. 6. Resistance vs temperature curves for 3D printed CB-PLA with different printing orientations: longitudinal (0°); oblique (45°/−45°); transverse (90°).

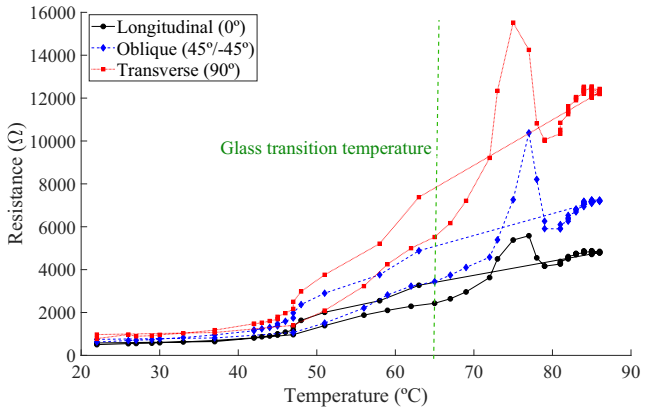

Fig. 7. Heating-cooling hysteresis resistance vs temperature curves for 3D printed CB-PLA with different printing orientations: longitudinal (0°); oblique (45°/−45°); transverse (90°).

the interfilament phases (contact region between deposited filaments) and their orientation with respect to the electric current direction. In this regard, a filament orientation along the current direction (longitudinal) favours the charge conduction and limits its resistance dependence on the quality of the sintering process between filaments. However, transverse orientations lead to filament-filament interphases along the current direction, making mechanical deformation (i.e., thermal expansion) highly susceptible to alter the resistive response of the sample.

To complete this analysis, we conducted a heating-cooling cycle test with the aim of identifying potential hysteresis in the resistance vs temperature curves. These results for the three different printing orientations are shown in Fig. 7. All these tests showed the same trend with a continuous decrease of the composite electric resistance when decreasing the temperature. Unlike during heating tests, less changes in the resistance-temperature slopes were observed. Therefore, it can be concluded that the resistance evolution with temperature differs during the cooling process with respect to the heating one. However, the initial electric resistance is mostly recovered at the end of the thermal cycle.

4. Interplay between mechanical and electrical responses

In this section we conducted a mechanical characterisation of both the 3D printed PLA 4043D and the 3D printed CB-PLA. Then, we performed an evaluation of the effects of mechanical deformation on electric resistance of the CB-PLA. The latter is analysed by means of variations in the overall electric resistance of the specimen. Therefore, the measurements do not account for spatial heterogeneities. According to the results presented in Section 3, the best and most homogeneous thermo-electrical behaviour is observed for the longitudinal printed specimens. In addition, there are numerous works in the literature that show a better mechanical performance for such a printing orientation [2,3,34]. Consequently, from this point we only focus on longitudinal specimens.

4.1. Mechanical characterisation

PLA is one of the most used materials for FDM due to its low melting temperature and minimal warping. In addition, PLA is a biodegradable, biocompatible material with good mechanical properties, being a perfect candidate from biomedical to electronic applications. The influence of 3D printing parameters on its mechanical behaviour has widely been studied in the literature [2,34], where specimens with a longitudinal orientation have shown the best mechanical response. Therefore, a mechanical characterisation was conducted on both PLA 4043D and CB-PLA specimens printed with longitudinal filaments orientation. To this end, we performed uniaxial tensile tests at quasi-static loading conditions with a number of tests per material equal to 4. These tests were conducted using a servo-hydraulic testing machine under displacement control at 1 mm/min, and with the incorporation of an extensometer to track strain values. The mean stress–strain curve for each material is shown in Fig. 8. As representative

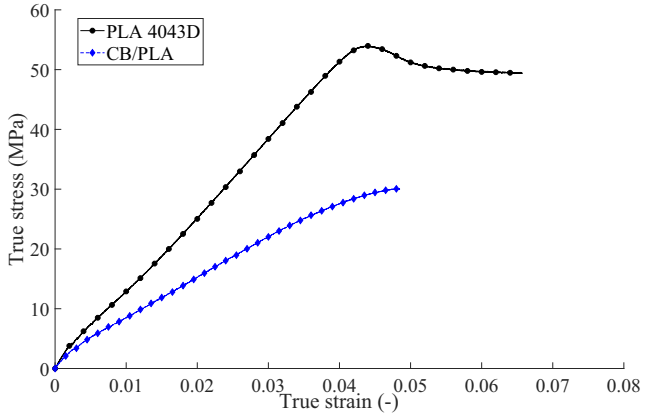

Fig. 8. Stress vs strain mean curves for 3D printed PLA and CB-PLA specimens with longitudinal (0°) printing orientation at quasi-static uniaxial tensile loading conditions.

properties we obtained a Young's modulus of 1.270 ± 0.037 GPa for the printed PLA and of 0.680 ± 0.042 GPa for the printed CB-PLA; while we obtained a yield stress of 55.10 ± 0.65 MPa for the printed PLA and of 30.80 ± 0.51 MPa for the printed CB-PLA. Counterintuitively, the PLA reinforced with the CB fibres presented lower mechanical properties by means of stiffness and yielding. To explain these results, we refer to Fig. 2, where it can be observed worse sintering between filaments and a higher porosity of the CB-PLA with respect to pure PLA. These features significantly impact the mechanical performance of the CB-PLA leading to a softer response and a loss in material ductility.

4.2. Mechanical deformation effects on composite resistance

In this section we explore the couplings between the mechanical and electric responses by means of deformation and electric conductivity. The assumption behind these tests is that the composite electric resistance directly depends on the physical formation of conductive electric paths and, therefore, a given mechanical deformation will play an important role in the disruption and new formation of such electric paths. To evaluate this mechano-electric coupling we developed an experimental setup composed of a universal testing machine that applies tensile loading to a printed CB-PLA specimen which is connected from both extremes to an Ohmmeter. Once again it must be remembered that the Ohmmeter will not heat the samples enough to modify their resistance. In addition, a recording camera is used to track the process. Thus, we obtained simultaneously the force-displacement curve along with measurements of variation of the material electric resistance. This setup is presented in Fig. 9. Note that we performed this analysis on longitudinal specimens to simplify the study as they provided the best thermo-electrical behaviour presenting no heterogeneities (see Section 3).

A representative set of results on a longitudinal specimen is shown in Fig. 10. Here, we observe the evolution of both the stress and the electric resistance as a function of the mechanical deformation (strain). A scheme of the mechano-electric conduction process during the deformation of the specimen is presented in a series of pictures in Fig. 10. In this regard, we conceptualised the printed specimen in a reference of initial state ("0" in Fig. 10) where the electric current can follow conductive paths formed by the aggregation of Carbon Black particles. As the specimen is stretched, some of these conductive paths break leading to an increase in electric resistance ("1" in Fig. 10). Within this region, the specimens present an averaged resistance versus longitudinal strain slope of $\frac{dR}{d\varepsilon} = 2156\ \Omega$. For larger deformations, this resistance-strain tendency is turned leading to a decrease of electric resistance with strain ("2" in Fig. 10). We hypothesise that this response can be explained by a contraction of the specimen in the transverse direction due to Poisson's ratio, which results into the formation of new conductive paths. Finally, if the deformation is increased, the electric resistance significantly increases with strain going to infinite as soon as the material reaches mechanical fracture ("3" in Fig. 10). Note that coupled to relative displacements of the conductive particles, changes in the specimen length/cross section area contributes to an increase in specimen's electric resistance.

5. Conclusions

This work evaluates the interplays between thermal, electrical and mechanical responses of 3D printed carbon black particles-PLA, CB/PLA manufactured by FDM. Three different printing configurations are considered according to the filament orientation: longitudinal (0°); transverse (90°); oblique (±45°) printing orientations.

- First, electro-thermal tests were conducted to evaluate the influence of electrical conductivity and conducted current on the sample temperature due to Joule heating. These results showed increments in temperature due to the resistive nature of the material and the associated Joule's effect. The distribution of such temperature increment depends on the filament printing direction. The longitudinal (0°) specimens showed a homogeneous distribution of temperature increase while it becomes more heterogeneous when increasing the printing angle with respect to the longitudinal orientation of the specimen geometry.
- Secondly, thermo-electrical tests were performed to analyse the influence of temperature on the DC resistance of the samples. These results showed lower resistance for longitudinal specimens and this resistance increases with the printing angle with respect to the longitudinal orientation of the specimen geometry. Moreover, all the printed specimens presented the same trends by means of resistance evolution with temperature: i) a plateau region where the electric resistance is almost constant; ii) a significant increase in resistance with temperature, that becomes stronger when reaching the glass transition of the polymeric matrix (65 °C); iii) a decrease of resistance with temperature after glass transition; iv) a final significant increase in resistance with temperature until reaching the disruption of conductive paths.
- Finally, mechano-electrical tests were carried out to analyse the effect of mechanical deformation on the specimens' resistance for longitudinal samples. These results showed an initial increase of resistance with longitudinal stretch, then this tendency turns into a decrease of resistance with longitudinal stretch (hypothesised as a consequence of Poisson's ratio effect) and, finally, a significant increase in resistance until complete rupture of the conductive paths.

Overall, these results contribute to the understanding of the physical interplays between mechanical, thermal and electrical processes in the behaviour of 3D printed CB/PLA composites. Future work will focus on the effect of applying an electric potential on the sample while deforming it and, therefore, the effect of the induced temperature on the mechanical response of the samples. These insights will provide new routes to design smart systems whose electric resistance or current depend on mechanical deformation on both magnitude and direction.

CRediT authorship contribution statement

I. Tirado-Garcia: Investigation, Methodology, Formal analysis, Writing - original draft. **D. Garcia-Gonzalez:** Investigation, Methodology, Formal analysis, Writing - original draft, Writing - review & editing, Funding acquisition. **S. Garzon-Hernandez:** Investigation,

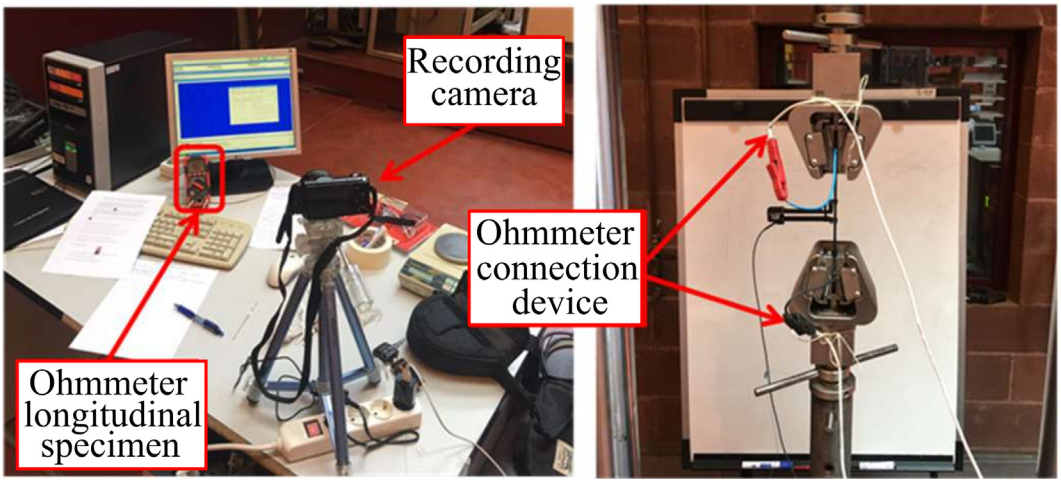

Fig. 9. Experimental setup for testing the influence of mechanical deformation on the resistance of 3D printed conductive specimens.

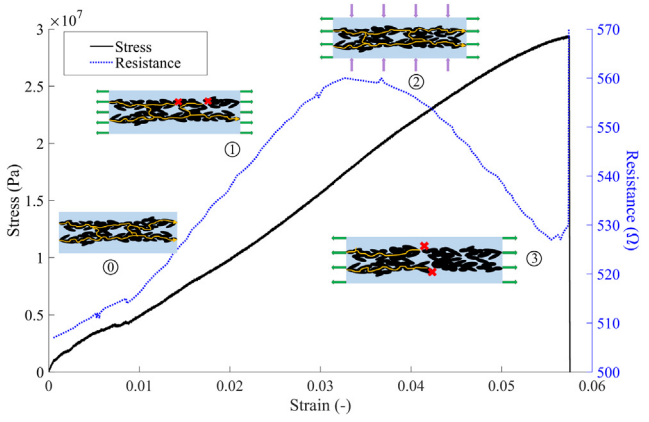

Fig. 10. Stress vs strain and resistance vs strain curves for a 3D printed CB-PLA with longitudinal (0°) printing orientation. The schematics of the deformation process stages are included where blue regions represent the polymeric matrix, black regions represent the conductive aggregates, orange lines represent conductive electric paths, and red crosses represent conductive paths' breaks due to mechanical deformation.

Methodology, Writing - original draft, Writing - review & editing. **A. Rusinek:** Investigation, Formal analysis, Writing - original draft, Writing - review & editing. **G. Robles:** Investigation, Methodology, Formal analysis, Writing - original draft. **J.M. Martinez-Tarifa:** Investigation, Methodology, Formal analysis, Writing - original draft, Funding acquisition. **A. Arias:** Investigation, Methodology, Formal analysis, Writing - original draft, Writing - review & editing, Funding acquisition.

Declaration of Competing Interest

The authors declare that they have no known competing financial interests or personal relationships that could have appeared to influence the work reported in this paper.

Acknowledgements

The authors acknowledge financial support from Ministerio de Ciencia, Innovación y Universidades, Spain, Agencia Estatal de Investigación y Fondo Europeo de Desarrollo Regional, Spain, under Grant number RTI2018-094318-BI00. D.G.-G., S.G.-H. and A.A. acknowledge support from Programa de Apoyo a la Realización de Proyectos Interdisciplinares de I + D para Jóvenes Investigadores de la Universidad Carlos III de Madrid (BIOMASKIN-CM-UC3M). D.G.-G. acknowledges support from the Talent Attraction grant (CM 2018 - 2018-T2/IND9992) from the Comunidad de Madrid, Spain. Some tests were made in the High Voltage Research and Test Laboratory (LINEALT) at UC3M.

References

[1] Duarte Ferreira A, Nóvoa P, Torres Marques A. Multifunctional Material Systems: A state-of-the-art review. Compos Struct 2016;15:3–35
[2] Garzon-Hernandez S, Garcia-Gonzalez D, Jerusalem A, Arias A. Design of FDM 3D printed polymers: an experimental-modelling methodology for the prediction of mechanical properties. Mater Design 2020;188.
[3] Garzon-Hernandez S, Arias A, Garcia-Gonzalez D. A continuum constitutive model for FDM 3D printed thermoplastics. Compos Part B 2020;201:15.
[4] Wegst UG, Bai H, Saiz E, Tomsia AP, Ritchie R. Bioinspired structural materials. Nat. Mater. 2015;14(1):23.
[5] Penumakala P, Santo J, Thomas A. A critical review on the fused deposition modeling of thermoplastic polymer composites Compos Part B B 2020;201:108336.
[6] Leigh SJ, Bradley RJ, Purssell CP, Billson DR, Hutchins DA, A simple, low-cost conductive composite material for 3D printing of electronic sensors, PLoS One 7 2012;11e49365.
[7] Deshmukh K, Houkan MT, AlMaadeed MA, Sadasivuni KK. Introduction to 3D and 4D printing technology: state of the art and recent trends. In 3D and 4D Printing of Polymer Nano Mater. Elsevier; 2020:1–24.
[8] Qian TT, Dong LIU, Tian XJ, Liu CM, Wang HM. Microstructure of TA2/TA15 graded structural material by laser additive manufacturing process. Trans. Nonferrous Metals Soc. China 2014;24(9):2729–36.
[9] Zhu C, Han TYJ, Duoss EB, Golobic AM, Kuntz JD, Spadaccini CM, Worsley MA. Highly compressible 3D periodic graphene aerogel micro lattices. Nat. Commun. 2015;6:696.
[10] Loo AH, Chua CK, Pumera M. DNA biosensing with 3D printing technology. Analyst 2017;142(2):279–83.
[11] Du Y, Chen J, Meng Q, Dou Y, Xu J, Biplab P, Per E. Flexible ternary carbon black/Bi2Te3 based alloy/polylactic acid thermoelectric composites fabricated by additive manufacturing. J Materiomics 2020;6:293–9.
[12] Gao B, Yang Q, Zhao X, Jin G, Ma Y, Xu F. 4D bioprinting for biomedical applications. Trends Biotechnol 2016;14:9.
[13] Joshi A, Goh JK, Goh KEJ. Polymer-based conductive composites for 3D and 4D printing of electrical circuits. In3D and 4D Printing of Polymer Nanocomposite Materials. Elsevier 2020:45–83.
[14] Du Y, Chen J, Meng Q, Dou Y, Xu J, Shen S. Thermoelectric materials and devices fabricated by additive manufacturing. Vacuum 2020;2178.
[15] Garcia-Gonzalez D, Garzon-Hernandez S, Rusinek A, Bernier R, Arias A. Low temperature mechanical behaviour of PVDF: cryogenic pre-treatment, quasi-static, cyclic and dynamic experimental testing and modelling. Mech Mater 2020;147.
[16] Garcia-Gonzalez D. Magneto-visco-hyperelasticity for hard-magnetic soft materials: theory and numerical applications. Smart Mater Struct 2019;28.
[17] Garcia-Gonzalez D, Landis CM. Magneto-diffusion-viscohyperelasticity for magneto-active hydrogels: rate dependences across time scales. J Mech Phys Sol 2020;139.
[18] Garcia-Gonzalez D, Hossain M. A microstructural-based approach to model magnetoviscoelastic materials at finite strains. Int J Sol Struct 2021;208:119–32.

[19] Hohimer C, Petrossiana G, Ameli A, Mo C, Pötschked P. 3D printed conductive thermoplastic polyurethane/carbon nanotube composites for capacitive and piezoresistive sensing in soft pneumatic actuators. Add Manuf 2020;34.
[20] Jayanth N, Senthil P. Application of 3D printed ABS based conductive carbon black composite sensor in void fraction measurement. Compos Part B 2019;159:224–30.
[21] Silva V, Fernandes-Junior W, Rocha D, Stefano J, Muñoz R, Bonacin J, Janegitz B. 3D-printed reduced graphene oxide/polylactic acid electrodes: a new prototyped platform for sensing and biosensing applications. Biosens Bioelect 2020;170.
[22] Alam F, Varadarajam K, Kumar S. 3D printed polylactic acid nanocomposite scaffolds for tissue engineering applications. Polym Test 2020;81.
[23] Yuk H, Lu B, Lin S, Qu K, Xu J, Luo J, Zhao X. 3D printing of conducting polymers. Natur Com 2020;11:1604.
[24] Inoue A, Yuk H, Lu B, Zhao X. Strong adhesion of wet conducting polymers on diverse substrates. SCI. Adv. 2020;6:394.
[25] Zhang C, Ma C, Wang P, Sumita M. Temperature dependence of electrical resistivity for carbon black filled ultra-high molecular weight polyethylene composites prepared by hot compaction. Carbon 2005;43:2544–53.
[26] Tan JC, Low HY. Embedded electrical tracks in 3D printed objects by fused filament fabrication of highly conductive composites. Add Manuf 2018;23:294–302.
[27] Spinellia G, Lambertia P, Tuccia V, Ivanovab R, Tabakovab S, Ivanov G, Kotsilkova R, Cimmino S, Di Maio R, Silvestre C. Rheological and electrical behaviour of nanocarbon/poly(lactic) acid for 3D printing applications Compos Part B 2019;167 467–476.
[28] Vaněčková E, Bouša M, Lachmanová S, Rathouský J, Gál M, Sebechlebská T, Kolivoška V. 3D printed polylactic acid/carbon black electrodes with nearly ideal electrochemical behaviour. J Electro Chem 2020;857.
[29] Garcia-Gonzalez D, Zaera R, Arias A. A hyperelastic-thermoviscoplastic constitutive model for semi-crystalline polymers: application to PEEK under dynamic loading conditions. Int J Plast 2017;88:27–52.
[30] Garcia-Gonzalez D, Garzon-Hernandez S, Arias A. A new constitutive model for polymeric matrices: application to biomedical materials. Compos Part B 2018;139:117–29.
[31] Kinvi-Dossou G, Matadi Boumbimba R, Bonfoh N, Garzon-Hernandez S, Garcia-Gonzalez D, Gerard P, Arias A. Innovative acrylic thermoplastic composites versus conventional composites: improving the impact performances. Compos Struct 2019;217–1:1–13.
[32] Barba D, Arias A, Garcia-Gonzalez D. Temperature and strain rate dependences on hardening and softening behaviours in semi-crystalline polymers: Application to PEEK. Int J Solids Struct 2020;182:205–7.
[33] Ahn S, Montero M, Odell D, Roundy S, Wright PK. Anisotropic material properties of fused deposition modeling ABS. Rapid Prototyping 2002;8(4):248–57.
[34] Chacón J, Caminero M, Núez P, a Plaza EG, a Moreno IG, Reverte J. Additive manufacturing of continuous fibre reinforced thermoplastic composites using fused deposition modelling: Effect of process parameters on mechanical properties. Compos Sci Technol 2019;181:07688.
[35] Ding S, Zou B, Wang P, Ding H. Effects of nozzle temperature and building orientation on mechanical properties and microstructure of PEEK and PEI printed by 3D-FDM. Polym Test 2019;78.
[36] Wang P, Zou B, Xiao H, Ding S, Huang C. Effects of printing parameters of fused deposition modeling on mechanical properties, surface quality, and microstructure of PEEK. J Mater Process Technol 2019;271:62–74.
[37] Stauffer D, Aharony A, Introduction to Percolation Theory 2014, second ed., Taylor & Francis Group, London.
[38] Abdalla A, Hamzah H, Keattch O, Covill D, Patel B. Augmentation of conductive pathways in carbon black/PLA 3D-printed electrodes achieved through varying printing parameters. Electro Acta 2020;354.
[39] Kim M, Sung D, Kong K, Kim N, Kim BJ, Wook H, Park YB, Jung M, Lee S, Kim S. Characterization of resistive heating and thermoelectric behavior of discontinuous carbon fiber-epoxy composites. Compos Part B 2016;90:37–44.
[40] Chen G, Rastak R, Wang Y, Yan H, Feig V, Liu Y, Jiang Y, Chen S, Lian F, Molina-Lopez F, Jin L, Cui K, Chung J, Pop E, Linder C, Bao Z. Strain- and Strain-Rate-Invariant Conductance in a Stretchable and Compressible 3D Conducting Polymer Foam. Matter 2019;1:205-218.
[41] Proto-Pasta. https://www.proto-pasta.com/pages/conductive-pla.
[42] Cardoso R, Rocha D, Rocha R, Stefeano J, Silva R, Richter Muñoz R. 3D-printing pen versus desktop 3D-printers: fabrication of carbon black/polylactic acid electrodes. Analyt Chim Act 2020;1132:10–9.
[43] Choi HJ, Kim M, Ahn D, Yeo S, Lee S. Electrical percolation threshold of carbon black in a polymer matrix and its application to antistatic fibre. Sci Rep 2019;9:6338.
[44] Jizhe W, Hongze L, Rongxuan L, Liangliang L, Yuan-Hua L, Ce-Wen N. Thermoelectric and mechanical properties of PLA/composite wires used for 3D printing. Compos Sci Technol 2018;157:1–9.
[45] Rocha D, Squissato A, da Silva S, Richter E. Munoz R. Improved electrochemical detection of metals in biological samples using 3D-printed electrode: Chemical/electrochemical treatment exposes carbon-black conductive sites. Electro Acta 2020;335:135688.
[46] Letcher T, Rankouhi B, Javadpour S. Experimental study of mechanical properties of additively manufactured ABS plastic as a function of layer parameters (2015), 10.1115/IMECE2015-52634.
[47] Rankouhi B, Javadpour S, Delfanian F, Letcher T. Failure analysis and mechanical characterization of 3D printed ABS with respect to layer thickness and orientation. J Failure Anal Prevent 2016;16(3):467–81.
[48] Croccolo D, Agostinis M, Olmi G. Experimental characterization and analytical modelling the mechanical behaviour of fused deposition processed parts made of ABS-M30. Comput Mater Sci 2013;79:506–18.
[49] Taherian R, Samiei Z. Investigation on electrical properties of polyvinyl acetate/graphite adhesive by joule heating and hall effect tests. Mater Today Communications 2020; 101680.
[50] Le T, Kim Y, Yoon H. Electrical and electrochemical properties of conducting polymers. Polymers 2017;9(4):150.
[51] Lu S, Wong P. Study on effect of Carbon Black on behavior of conductive polymer composites with positive temperature coefficient. IEEE Trans Compon Packag Technol 2000;23:1.